OPTICAL REVIEW Vol. 18, No. 2 (2011) 197–202

New Temporal High-Pass Filter Nonuniformity Correction Based on Bilateral Filter

Chao ZUO*, Qian CHEN, Guohua GU, and Weixian QIAN

440 Lab, JGMT, EEOT, Nanjing University of Science and Technology, Nanjing 210094, China

(Received September 26, 2010; Accepted December 27, 2010)

A thorough analysis of low convergence speed and ghosting artifacts in temporal high-pass filter correction has been undertaken in this paper and it has found out that the keys of these problems are the interference of a large sum of unrelated scene information in the nonuniformity correction (NUC) process. In order to overcome these drawbacks, a new scene-based NUC technique based on bilateral filter has been developed. This method separates the original input frames into two parts and it estimates the NUC parameters only by using the residuals. The experimental results have shown that it can significantly increase convergence speed and reduce ghosting artifacts.

Keywords: infrared focal plane array, nonuniformity correction, ghosting artifacts, bilateral filter, convergence speed

1. Introduction

With the development of the infrared focal-plane array (IRFPA) technology, the infrared imaging systems have been widely applied in the fields of military, astronomy, industry and so on. However, it is known to all that the sensitivity of the infrared focal-plane array is greatly influenced by the fixed-pattern noise (FPN), i.e., the nonuniformity, which is generated by the IRFPA's different responses to the same input signal.[1,2] In order to solve this problem, the algorithm for nonuniformity correction (NUC) should be applied.

NUC techniques can be classified into two categories: calibration-based technique and scene-based technique. The most well-known calibration-based NUC method is the two-point correction, which employs two blackbodies at two different known temperatures around the operation point in order to estimate gain and offset related to each detector of the IRFPA.[3] Unfortunately, the nonuniformity is always influenced by such external conditions as ambient temperature, variation in the transistor bias voltage and the time-dependent nature of the object irradiance. All these factors have made each detector of the focal plane drift slowly with the time lapse.[4] Therefore, these calibration-based NUC methods require the procedure to be periodically performed so as to guarantee the correction of the temporal drift of the FPN. To make up for the inconvenience, many scene-based nonuniformity correction (SBNUC) techniques have been proposed. Extensive studies and applications of temporal high-pass filter technique (THPF-NUC),[2,5] constant statistics method (CS-NUC),[6] and neural-network-based nonuniformity correction (NN-NUC)[2] have been conducted because of their relatively lower computational complexity, smaller storage demands, and better real-time performance.

Almost all SBNUC algorithms are faced with one serious problem: ghosting artifacts. When motion across the whole image or part of it temporarily slows or halts, the static objects will blend in the correction parameters. When motion resumes, the old scene superimposed on the new "corrected" scene. A number of researchers have done a lot of work that deal with the problem of ghosting. Harris and Chiang[7] developed a strategy to eliminate ghosting artifacts in the CS-NUC method by employing a change threshold to gate the update of the statistical parameter estimates. Vera and Torres[8] proposed an enhanced version of the NN-NUC based on a learning-rate adaptively updated using the data themselves. Qian[9] presented a deghosting technique in the THPF-NUC where the correction coefficients are calculated by using only the high space-frequency part of the image.

This paper mainly analyzes the root cause of the occurrence of low convergence speed and ghosting artifacts in the THPF-NUC method and it has pointed out that the this phenomenon is primarily caused by the interference of the unrelated scene information in the NUC process. As a result, the THPF-NUC algorithm has been modified to alleviate the effects of the ghosting artifacts and improve the convergence speed. This improved THPF-NUC algorithm is based on the division of the raw image into two parts using of an edge-preserving nonlinear spatial filter that replaces the average filter proposed by Qian.[9] The basic idea of this algorithm is to eliminate the base part and the edges in the scene which are the main responsibilities of low convergence speed and the residuals are used to estimate the FPA's nonuniformity. In this way, improvement in convergence speed can be achieved and effective removal of ghosting artifacts can be attained.

This paper is organized as follows. In §2, a brief review of the THPF-NUC algorithm is given and the concrete causes of ghosting are analyzed. In §3, the image separation methods using average filter and bilateral filter are compared, and a new bilateral filter based temporal high-pass filter NUC (BFTH-NUC) is presented. In §4, experimental results are displayed. Finally, there comes the conclusion in §5.

*E-mail address: surpasszuo@163.com

2. THPF-NUC and Its Problems

2.1 THPF-NUC algorithm

It is held in the THPF-NUC[2,5] that high-frequency information belongs to the scene while low-frequency information belongs to fixed pattern noise when studying each pixel over time. Hence, estimates of the FPN can be obtained by low-pass filtering the image sequence along the temporal axis. NUC can be achieved when the estimate of FPN is subtracted. The whole process resembles a temporal high-pass filter. A temporal average $f(n)$ of the image sequence is generated by a recursive IIR filter and subtracted from the current frame $x(n)$

$$y(n) = x(n) - f(n), \tag{1}$$

where

$$f(n) = \frac{1}{M}x(n) + \left(1 - \frac{1}{M}\right)f(n-1). \tag{2}$$

Here x is the input frame and y is the output of correcting, n is frame index. M is the time constant of filter.

2.2 Convergence speed and ghosting artifacts

In most cases, the THPF-NUC method is just a simple and effective way to correct the FPN, but it has two shortcomings: being motion dependent and sensitive to extreme scene,[2] i.e., if there are insufficient random motions or excessively strong scene values in the frames, the processor will essentially fade out the stationary image and affect the convergence process. A burn-in effect still comes out even if the extreme values will not stay long.

Nonrandom motion includes insufficient global motion, local motion, directed motion, etc. If some part of the scene remains motionless for several algorithm iterations, it will be considered to be fixed pattern noise and be blended into the background. When this part continues its motion, it will leave an inverse ghost image in its original place. Besides, ghosting artifacts may occur when the image motion is one-direction-oriented. For example, a view of ghost image may be generated when the sensor suddenly changes its horizontal motion into a vertical one.

Extreme scene values also affect the convergence speed seriously. Although the scene may be in continuous movement, the extreme values will also leave ghosting-like artifacts due to their high digital levels, which have a greater effect on correction parameters than other parts.

The ghosting caused by insufficient global motion can be reduced by the change detection mechanism which halts the updating of the correction parameters when motion of the scene is insufficient. However, this method is useless for ghosting in other situations. It is known to all that it is the infrared photon flux collected by the detector that is the main reason for the changes of FPA's response when compared to the FPN and the temporal noise. Therefore, the dynamic range of the scene irradiation is much greater than that of the noise. If all parts of the raw image are used to estimate the nonuniformity, the correction will be very susceptible to external irradiation because of the great sum of scene information, especially the "strong" objects contained in the raw image frames. For example, when an object with strong irradiation enters the scene, the correction coefficients in the object region will increase dramatically, making the object gradually "melt" into the background. When it leaves its original position, a reverse ghost image will appear owing to skew offset estimation and the normal convergence process will be seriously affected.

From the previous analysis, it is stated that the root cause of low convergence speed and ghosting artifacts in the THPF algorithm lies in the interference of the amount of unrelated scene information in the NUC process. Thus, if scene information from the original image can be erased as much as possible, especially the strong objects, and the residual part can be used to estimate nonuniformity parameters. By combining these together can the adverse effects of non-random motion and strong scene values be minimized. In this way, the speed of convergence can be increased and ghosting artifacts can be reduced. Therefore, the biggest problem now is how to separate the noise from the scene effectively.

3. Bilateral Filter Based Temporal High-Pass Filter NUC

3.1 Image separation based on bilateral filter

The simplest method of image separation is to use a linear low-pass filter to separate the image into two parts: low spatial frequency (LSF) and high spatial frequency (HSF). The LSF of the image includes most scene information while the HSF contains most noise. According to this theory, Qian put forward a NUC algorithm called space low-pass and temporal high-pass (SLTH),[9] which uses an average filter to divide the space frequency into two parts and only process the HSF part of the non-uniformity. The algorithm can be expressed as follows:

$$y(n) = x(n) - f(n), \tag{3}$$

where

$$f(n) = \frac{1}{M}X^{\mathrm{HSF}}(n) + \left(1 - \frac{1}{M}\right)f(n-1), \tag{4}$$

$$x^{\mathrm{HSF}}(n) = x(n) - x^{\mathrm{LSF}}(n) = x(n) - x(n) \otimes A. \tag{5}$$

$$X_{ij}^{\mathrm{HSF}} = \begin{cases} x_{ij}^{\mathrm{HSF}} & |x_{ij}^{\mathrm{HSF}}| < Th \\ 0 & |x_{ij}^{\mathrm{HSF}}| \geq Th \end{cases} \tag{6}$$

A is an average filter and $\otimes$ is a convolution operator. Since average filtering is an average of the intensity of the adjacent positions, so it is impossible to distinguish the noise from the edge of the scene. In this way, a threshold value is introduced. If a pixel's x_{ij}^{HSF} is larger than Th, the pixel will be considered as the edges of the scene and won't be involved in the calculation of correction parameters. SLTH-NUC to a great degree has made up for the THPF-NUC's deficiency since it only handles the HSF of the raw image. This method improves the convergence speed and considerably reduces the ghosting artifacts. Nevertheless, there are three problems existing in the separation method based on average filter with a threshold:

1) It is difficult to find a proper threshold to separate the edges of the scene features and the noise. A lager threshold will lead some strong edges in the scene to the HSF part, which will affect the convergence speed. Conversely, a lower threshold will not be able to remove the nonuniformity efficiently.
2) The HSF part of image obtained by linear filters will lead to halo artifacts[10] where large intensity variations are present and they can also affect the convergence speed and generate "ghost contours".
3) If the HSF parts which are larger than the threshold are set to zero, these parts will not participate in the calculation of nonuniformity. However, the nonuniformity of these positions still exists. If the HSF of some parts of an image exceeds the threshold by several frames, the corresponding nonuniformity parameters will not get updated for long and get smaller. Therefore, the nonuniformity will gradually reappear in the corresponding part of the image.

To overcome the shortcomings of the linear filters, many nonlinear filters[11,12] have been proposed. Bilateral filter was developed by Tomasi and Manduchi[12] as an alternative to anisotropic diffusion.[11] It is a nonlinear filter whose output is a weighted average of the input. Similar to the Gaussian convolution, the bilateral filter is also defined as a weighted average of pixels. But the difference is the bilateral filter has taken the variation of intensities into account to preserve edges. The rationality of bilateral filtering lies in its decision of the resemblance of two pixels, which tests whether their spatial distance is close enough and whether their intensity values are similar enough. When an input image I is given, the output of the bilateral filter for a pixel (i, j) is

$$I^{\mathrm{BF}}(x,y) = \frac{\sum_{(i,j)\in S_{x,y}} w(i,j)I(i,j)}{\sum_{(i,j)\in S_{x,y}} w(i,j)}. \tag{7}$$

The total mask of the weights $w(i, j)$ is obtained from the product of two different masks in the spatial and intensities domains as $w_s(i, j)$ and $w_r(i, j)$ respectively

$$w_s(i,j) = \exp\left\{-\frac{d_s^2\{(i,j),(x,y)\}}{2\sigma_s^2}\right\} = \exp\left\{-\frac{(i-x)^2+(j-y)^2}{2\sigma_s^2}\right\}, \tag{8}$$

$$w_r(i,j) = \exp\left\{-\frac{d_r^2\{(i,j),(x,y)\}}{2\sigma_r^2}\right\} = \exp\left\{-\frac{\{I(i,j)-I(x,y)\}^2}{2\sigma_r^2}\right\}, \tag{9}$$

hence,

$$w(i,j) = w_s(i,j)\cdot w_r(i,j), \tag{10}$$

where σ_s and σ_r are two standard deviation parameters defining the extension of the two Gaussian kernel. It can be observed that the weights depend on both the Euclidean distance $d_s\{(i, j), (x, y)\}$ and difference in intensity value $d_r\{(i, j), (x, y)\}$. The bilateral filter is controlled by σ_s and σ_r, which control the decay of the two weight factors. As the range parameter σ_r increases, the bilateral filter becomes closer to Gaussian blur. When both two parameters are large enough, the bilateral filter will be changed to an average one.

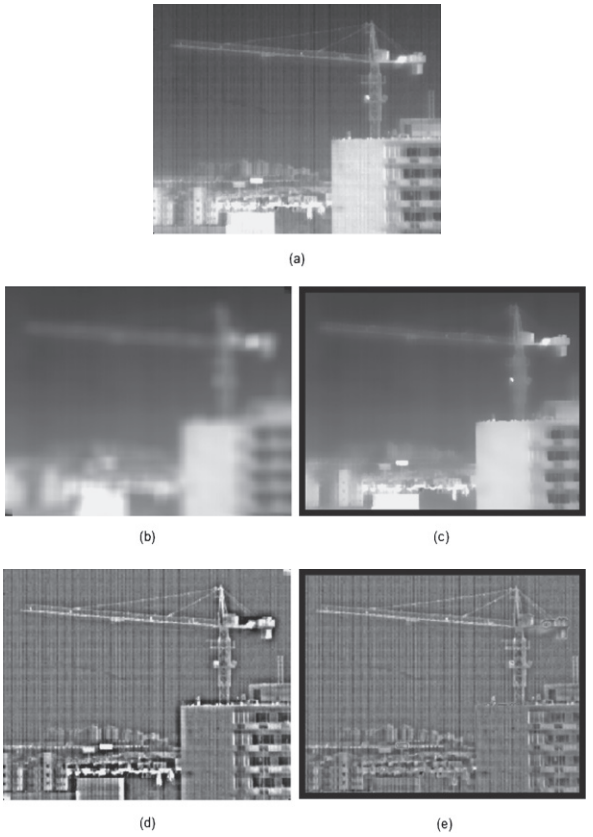

Fig. 1. Image separation results. (a) Uncorrected infrared image. (b) Output of the average filter ($D = 15$). (c) Residual of the average filter. (d) Output of the bilateral filter ($D = 15$, $\sigma_s = 2.5$, $\sigma_r = 130$). (e) Residual of the bilateral filter.

Figure 1(a) shows an uncorrected infrared image, serious striping effects are shown and it is probably caused by the readout electronics. The output of the average filter (filter size $D = 15$ pixels) and its residual are shown in Figs. 1(b) and 1(c), while the output of the bilateral filter (filter size $D = 15$ pixels, $\sigma_s = 2.5$, $\sigma_r = 130$) and its residual are shown in Figs. 1(d) and 1(e). The perfect situation for the separation task is that only noise and the nonuniformity are contained in the residual. Nevertheless, besides the noise, the residual after average filtering contains most of the edges in the scene and the obvious halo artifacts around the strong edges. Bilateral filter yields a more acceptable result because the edges visible in the residual are much fainter and there is no halo artifact.

To illustrate it in a simplified manner, a row of the 1D signal [Fig. 2(a)] has been extracted to represent the pixels' digital levels along the row 195 of the IR images shown in Fig. 2(b). This row is a nice example because of its containing of large signal variations, strong edges of the structures and enough strip nonuniformity. From Figs. 2(c) and 2(d), it can be observed that most of the noise and

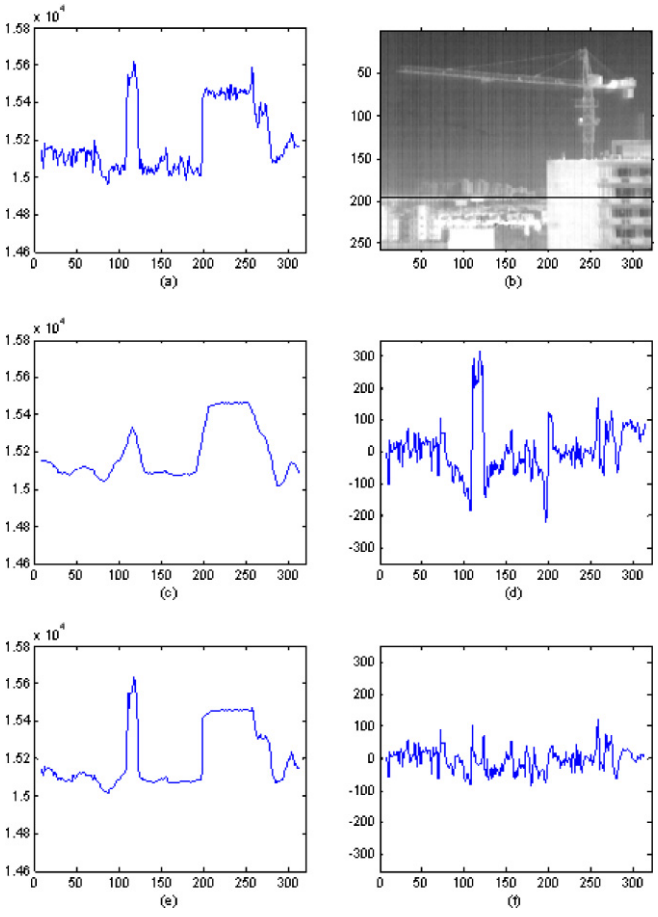

Fig. 2. (Color online) Row 195 [indicated in (b)] filtering results. (a) Raw infrared signal. (c) Output of the average filter ($D = 15$). (d) Residual of the average filter. (e) Output of the bilateral filter ($D = 15$, $\sigma_s = 2.5$, $\sigma_r = 130$). (f) Residual of the bilateral filter.

nonuniformity (represented by small fluctuations) can be filtered to the residual effectively through average filtering, but the strong edges of the image (represented by steep zooms or drops) become much smoother, and the height of narrow peak in Fig. 2(a) (caused by a billboard's sunlight reflection) is reduced a lot in Fig. 2(c), which becomes ripples and peaks in the corresponding area in Fig. 2(d). A threshold value between 100 and 150 can be used to truncate the residual, but there still remain some peaks and ripples close to the threshold that can not be effectively removed. If a smaller threshold is used, the separation result will be affected because of the exclusion of some high spatial frequency nonuniformity from the residual. From Figs. 2(e) and 2(f), the strong edges of the scene are excluded from the residual of bilateral filter to make most of it tiny details of the image, most of noise and nonuniformity included. Therefore, a more stable and accurate estimation can be obtained by using the residual of bilateral filter to calculate the NUC parameters.

3.2 *Bilateral filter based temporal high-pass filter NUC*

As is discussed from the above, most scene information and strong edges can be excluded from the residual effectively by the bilateral filter. Moreover, quicker convergence and fewer ghosting artifacts can be obtained by only processing the residual. So the algorithm is expressed as follows:

$$y(n) = x(n) - f(n), \tag{11}$$

where

$$f(n) = \frac{1}{M} x^{\mathrm{BFr}}(n) + \left(1 - \frac{1}{M}\right) f(n-1), \tag{12}$$

$$x^{\mathrm{BFr}}(n) = x(n) - x^{\mathrm{BF}}(n). \tag{13}$$

Here x is the input frame, y is the output of correcting, and n is frame index. $x^{\mathrm{BF}}, x^{\mathrm{BFr}}$ represent the output of bilateral filter and the residual. Referring to §3.1, it is known that there are two parameters controlling the behavior of the bilateral filter, σ_s and σ_r, representing the spatial and intensity domain behaviors respectively. The spatial parameter σ_s can be chosen according to the spatial frequency feature of the device's nonuniformity. The typical size of bilateral filter is $D = 15$, and $\sigma_s = 2.5$ to keep the Gaussian effect. The choice of the range parameter σ_r is more crucial. It has to take the level of nonuniformity into consideration, and this can be measured in the laboratory. In order to obtain the best performance, the σ_r can be set as 2 to 4 times of the standard deviation of the nonuniformity.

3.3 *Convergence*

In this section, a mathematical analysis is undertaken, which explains the reason why the proposed algorithm can converge faster than the THPF-NUC and SLTH-NUC. As a recursive equation is adopted to estimate the true value of nonuniformity offset, eq. (2) can be rewritten as follows:

$$\hat{m}_x(n) = \frac{1}{M} x(n) + \left(1 - \frac{1}{M}\right) \hat{m}_x(n-1), \tag{14}$$

where $\hat{m}_x(n)$ is the estimated offset which replaces the $f(n)$ in eq. (2). The mean-square error (MSE) of the recursive nonuniformity offset estimation can be written as

$$\begin{aligned} \mathrm{MSE}(n) &= E[(\hat{m}_x(n) - m)^2] \\ &= \frac{1}{M^2} E[(x(n) - m)^2] \\ &\quad + \frac{2(M-1)}{M^2} E[(x(n) - m)(\hat{m}_x(n-1) - m)] \\ &\quad + \left(1 - \frac{1}{M}\right)^2 E[(\hat{m}_x(n-1) - m)^2], \end{aligned} \tag{15}$$

where $E[\cdot]$ is statistical expectation operator, m is the true nonuniformity offset. If the scene in continuous movement, the signals of each pixel along the temporal axis $x(n)$ can be viewed as a group of independent and identically distributed random variables. So $x(n)$ and $\hat{m}_x(n-1)$ are statistically independent, and the second part of eq. (15) can be rewritten to

$$\begin{aligned} &\frac{2(M-1)}{M^2} E[(x(n) - m)(\hat{m}_x(n-1) - m)] \\ &\quad = \frac{2(M-1)}{M^2} (E[x(n)] - m) E[\hat{m}_x(n-1) - m]. \end{aligned} \tag{16}$$

Based on constant statistics constraint,[6] the true nonuniformity offset m should be equal to $E[x(n)]$. Thus

$$\frac{2(M-1)}{M^2}(E[x(n)]-m)E[\hat{m}_x(n-1)-m]=0. \quad (17)$$

So eq. (15) can be simplified to

$$\begin{aligned}\mathrm{MSE}(n) &= \frac{1}{M^2}E[(x(n)-m)^2] \\ &\quad + \left(1-\frac{1}{M}\right)^2 E[(\hat{m}_x(n-1)-m)^2] \\ &= \frac{1}{M^2}\sigma_x^2 + \left(1-\frac{1}{M}\right)^2 \mathrm{MSE}(n-1),\end{aligned} \quad (18)$$

where σ_x is the standard deviation of $x(n)$. Equation (18) is recursive and can be traced back to

$$\begin{aligned}\mathrm{MSE}(n) &= \frac{1}{2M-1}\left[1-\left(1-\frac{1}{M}\right)^{2n}\right]\sigma_x^2 \\ &\quad + \left(1-\frac{1}{M}\right)^{2n}\mathrm{MSE}(0),\end{aligned} \quad (19)$$

where MSE(0) is the initial error of the offset which depends on the initial value of $\hat{m}_x(0)$, if we use eq. (12) instead of eq. (2):

$$\begin{aligned}\mathrm{MSE}^{\mathrm{BFr}}(n) &= \frac{1}{2M-1}\left[1-\left(1-\frac{1}{M}\right)^{2n}\right]\sigma_{x^{\mathrm{BFr}}}^2 \\ &\quad + \left(1-\frac{1}{M}\right)^{2n}\mathrm{MSE}^{\mathrm{BFr}}(0).\end{aligned} \quad (20)$$

Similarly, in SLTH-NUC, the MSE of the HSF of the offset can be rewritten as:

$$\begin{aligned}\mathrm{MSE}^{\mathrm{HSF}}(n) &= \frac{1}{2M-1}\left[1-\left(1-\frac{1}{M}\right)^{2n}\right]\sigma_{x^{\mathrm{HSF}}}^2 \\ &\quad + \left(1-\frac{1}{M}\right)^{2n}\mathrm{MSE}^{\mathrm{HSF}}(0).\end{aligned} \quad (21)$$

It has been noted that the second parts of the three equations are only related to M and exponentially decrease from initial error to zero as n increases. Only the first parts which dominate the MSE when n is large enough are discussed. It can be seen that the first parts are in proportion to σ_x^2, $\sigma_{x^{\mathrm{HSF}}}^2$, and $\sigma_{x^{\mathrm{BFr}}}^2$, and it means smaller standard deviation is, the faster and more precise the convergence will be. As is mentioned in §3.1, the $\sigma_{x^{\mathrm{BF}}}^2$ is much smaller than the corresponding $\sigma_{x^{\mathrm{HSF}}}^2$ and σ_x^2 under the same condition. Therefore in order to reach the same error of offset estimate, the proposed method needs fewer samples than the THPF-NUC and SLTH-NUC.

4. Experimental Procedure

In this section, the proposed BFTH-NUC is tested with infrared data corrupted with simulated nonuniformity. The infrared sequences with artificial nonuniformity are generated from a clear 2000 frame infrared video sequence, and the corrupted video sequences are obtained by using a synthetic offset with a zero-mean Gaussian distribution with a standard deviation of 50. For the first 80 frames, the camera moves in a steady and consistent manner in prevention of any burn-in. Then, the camera will be moved more slowly and towards a more complicated scene. Around Frame 850, the camera is shifted to a scene with many extreme values caused by sunlight reflection. After frame 1650, the scene motion is increased and the extreme scene goes away.

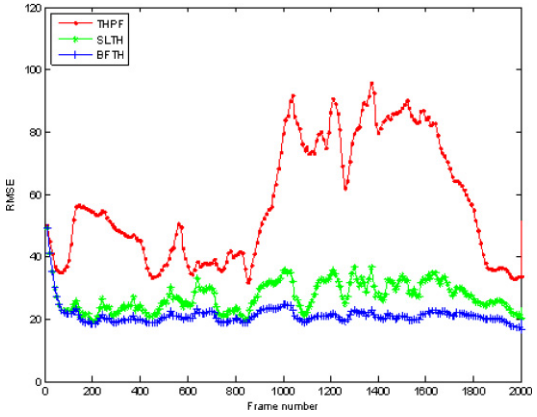

Fig. 3. (Color online) RMSE versus frame number for the three SBNUC algorithms.

The following three algorithms are compared in detail: the THPF-NUC, SLTH-NUC and the BFTH-NUC proposed in this text. The setting of the time constant M of all three algorithms is 33 and the space low-pass and temporal high-pass NUC algorithm uses a threshold of $Th = 150$. Meanwhile, the BFTH uses $D = 15$, $\sigma_s = 2.5$, $\sigma_r = 150$. The root-mean-square error (RMSE) can be adopted for measurement to have an objective evolution of the correction performance of a certain NUC algorithm. RSME is defined as follows:

$$\mathrm{RMSE} = \sqrt{\frac{1}{M\times N}\sum_{i,j}(I_{ij}-\hat{I}_{ij})^2}, \quad (22)$$

where I_{ij} is the (i,j) pixel value of the true frame while $\hat{I}_{ij}$ is (i,j) the pixel value of the corrected frame. M and N are respectively the rows and columns of the image. The RMSE versus frame numbers of the three SBNUC algorithms are shown in Fig. 3. Figures 4 and 5 show the images of Frame 130 (slow motion) and Frame 1370 (extreme scene). Figures 4(a) and 5(a) show the true radiance of the scene. The images corrupted with simulated nonuniformity are shown in Figs. 4(b) and 5(b). The outputs using the THPF, SLTH, and BFTH are shown in Figs. 4(c)–4(e), and Figs. 5(c)–5(e) respectively.

It can be noted from Fig. 3 that the SLTH method and BFTH method significantly outperform the THPF method due to their faster convergence speed and lower RMSE. In the first 80 frames, as the global motion is adequate and the scene is not very complicated, the curves of all the three algorithms have a stable falling tendency. Among the falling curves, the speed of the BFTH algorithm takes the lead and its RMSE falls to 21.94 at the 80th frame. When the global motion slows down, serious ghosting artifacts appear in THPF's output [Fig. 4(c)], meanwhile its RMSE bounce above the initial value. In SLTH's output, some ghost

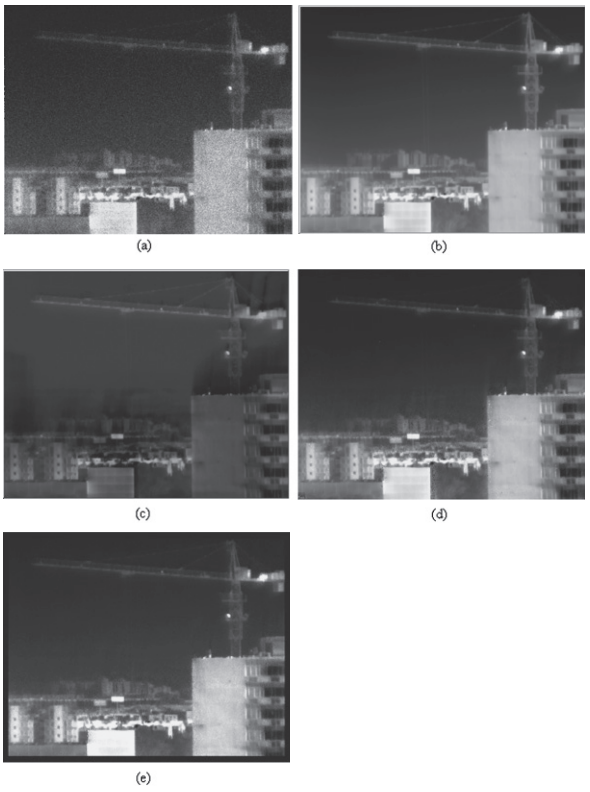

Fig. 4. Frame 130 in the sequence. (a) Image with simulated offset nonuniformity. (b) Uncorrupted image. (c) Corrected with the THPF. (d) Corrected with the SLTH. (e) Corrected with the BFTH.

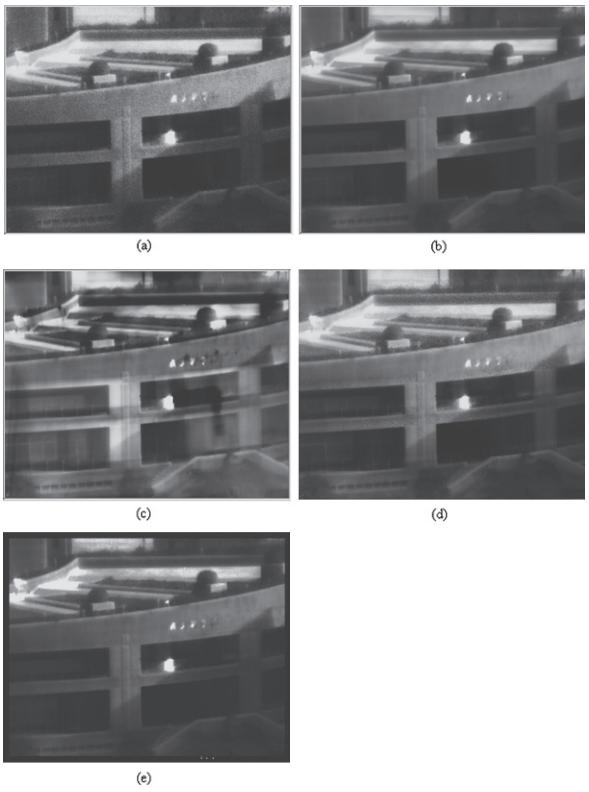

Fig. 5. Frame 1310 in the sequence. (a) Image with simulated offset nonuniformity. (b) Uncorrupted image. (c) Corrected with the THPF. (d) Corrected with the SLTH. (e) Corrected with the BFTH.

contours are also visible [Fig. 4(d)], which makes its RMSE curve fluctuate to a large degree. However, we can hardly see any ghost artifact in the BFTH's output [Fig. 4(e)] and the curve of its RMSE has shown the most stable tendency. When the extreme objects enter into the field of view, the RMSE of THPF suddenly rises above 90. The severe ghosting artifacts deteriorate the image and make it difficult to be observed normally [Fig. 5(c)]. The SLTH's RMSE also rebounds to 33.62. Besides, the nonuniformity reappears around the neighborhood of the strong edges due to the algorithm's threshold cutout as analyzed in §3.1 [Fig. 5(d)]. While the BFTH still can keep a good output [Fig. 5(e)] and a lower RMSE. From the above experimental results, it can be concluded that BFTH has the fastest speed of convergence and the most stable error during the whole process. Moreover, only through the correction of BFTH can the ghosting artifact be erased. Without considering the base component of nonuniformity, the RMSE of BFTH keeps around 20, and reaches 16.91 at the last frame.

5. Conclusions

In this paper, the main reasons for the problems in the THPF-NUC are discussed and it is concluded that the scene information of the image should be eliminated from the calculation of NUC coefficients as much as possible. Based on this analysis, a new NUC method called BFTH has been proposed, which adopts a bilateral filter to divide the input frame into two components and only the residual is used to estimate the NUC coefficients. The separation based on bilateral filter gives a more accurate estimation of FPN than the one based on linear filter due to its edge-preserving characteristic. Experiments have shown that the proposed method offers the best performance when compared to any other methods tested. Moreover, its ability to avoid the production of ghosting artifacts is pretty impressive.

References

1) D. A. Scribner, M. Kruer, and J. Killiany: Proc. IEEE **79** (1991) 66.
2) D. A. Scribner, K. A. Sarkady, J. T. Caulfield, M. R. Kruer, G. Katz, and C. J. Gridly: Proc. SPIE **1308** (1990) 224.
3) A. Friedenberg and I. Goldbatt: Opt. Eng. **37** (1998) 1251.
4) O. Riou, S. Berrebi, and P. Bremond: Proc. IEEE **5405** (2004) 294.
5) D. A. Scribner, K. A. Sarkady, and J. T. Caulfield: Proc. IEEE Int. Conf. Neural Networks, 1993, p. 1955.
6) J. G. Harris and Y. M. Chiang: IEEE Trans. Image Process. **8** (1999) 1148.
7) J. Harris and Y. Chiang: Proc. SPIE **3377** (1998) 106.
8) E. Vera and S. Torres: in Proc. of Int. Conf. Image Processing (ICIP), Vol. 3, 2003, p. 1001.
9) W. Qian, Q. Chen, and G. Gu: Opt. Rev. **17** (2010) 24.
10) F. Branchitta, M. Diani, G. Corsini, and M. Romagnoli: Opt. Eng. **48** (2009) 096401.
11) J. Tumblin and G. Turk: Proc. ACM SIGGRAPH **99** (1999) 83.
12) Tomasi and R. Manduchi: IEEE Proc. 6th Int. Conf. Computer Vision, Bombay, 1998, p. 839.